

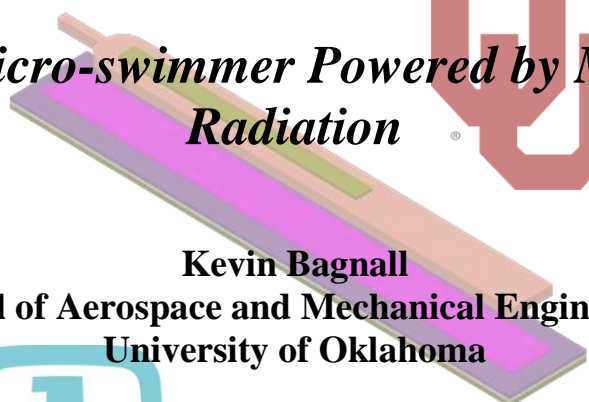
**Sandia National Laboratories  
University Alliance Design Competition  
Novel Design Category**

***MEMS Micro-swimmer Powered by Microwave  
Radiation***

**Kevin Bagnall  
School of Aerospace and Mechanical Engineering  
University of Oklahoma**

**Faculty Advisor: Dr. Harold Stalford**

**May 19, 2009**



## **I. Abstract**

This whitepaper presents the design of a novel MEMS micro-swimmer and micro-fluidic environment using the SUMMiT V™ fabrication process. This design is the first known micro-scale artificial swimmer capable of being produced by a batch surface micromachining process. The swimmer is propelled by the oscillatory motion of a tail similar to planar flagella used by bacteria and mammalian spermatozoa. Travelling waves are produced by the cyclic heating of an aluminum-polysilicon bimorph strip. Microwave rays incident on the aluminum surface result in high temperature changes due to inductive heating near the surface. The bimorph strip bends because of the large difference in the coefficient of thermal expansion between the two materials. The micro-swimmer is initially attached to the chip and is released after fabrication by several mechanical and thermal mechanisms. The basic proposed micro-swimmer design has a tail length and width of 100  $\mu\text{m}$  and 10  $\mu\text{m}$  respectively. Several micro-swimmers will be fabricated inside a sealed micro-lake, a sealed micro-stream channel, and an open micro-lake for convenient experimentation. To further research in the area of micro-swimmers and microwave powered actuators, several experimental polysilicon-aluminum actuators were designed. Coupled transient structural-thermal simulations performed in ANSYS show that the basic micro-swimmer tail is capable of producing an oscillatory motion with beat amplitude of 0.49  $\mu\text{m}$  and frequency of 5 Hz and predicted swimming speed of 4.1  $\mu\text{m/s}$ . This design represents a creative and innovative use of the SUMMiT V™ process and will serve as a fascinating educational demonstration for K-12 and post-secondary students.

## **II. Objective**

The objective of this design was to develop a novel micro-swimmer remotely powered by microwave radiation and demonstrate its operation in a micro-fluidic environment. The design includes several types of spermatozoa-like micro-swimmers, a micro-fluidic lake and stream channel, and experimental actuators. In addition to the micro-swimmer, the design is aimed to study the behavior of polysilicon-aluminum bimorph actuators excited by microwave radiation.

## **III. Introduction**

Although MEMS devices have been fabricated with surface micromachining processes since the 1980s, the field of micro-robotics is a continually expanding frontier for MEMS development. Since the advent of micro- and nanotechnology, scientists and science fiction authors have envisioned small robots capable of travelling inside the human body for medical research and treatment. Micro-scale robots of the future may be capable of performing medical procedures that are too intricate or that affect areas too sensitive to be performed by a human surgeon. In addition, micro-swimming robots carrying cargo may be able to deliver drugs to the brain without having to be taken orally and metabolized by the body. Precise drug delivery to the nervous system could potentially increase the effectiveness of pharmaceuticals and decrease the cost of drug development in the coming years.

In the mid 1990s, researchers in Japan introduced a millimeter scale swimmer propelled by fins and piezoelectric actuators [8-9]. The proposed applications for the swimmer included biomedicine and industrial non-destructive pipe evaluation. The authors designed mechanisms

to propel and steer the swimmer and obtained experimental results with an actual fabricated device. However, the approximately 50 mm length of the swimmer made it impractical for biomedical applications within the human body. Photographs of the swimmer developed in Japan are shown in Figure B2.

More recently, researchers have been developing microscopic swimming devices by linking paramagnetic beads and manipulating the beads in an oscillating magnetic field [7, 16]. The presence of an alternating magnetic field causes the doublets, quadruplets, or strings of beads to rotate and propel the swimmer like a helical bacterial flagellum. Doublets created by *Tierno et al. (2008)* were observed to obtain swimming speeds up to 3  $\mu\text{m/s}$  [16]. Researchers were able to direct the doublet bead swimmers to follow a rectangular path in a micro-fluidic channel by adjusting the external magnetic field. Images of an individual magnetic doublet and multiple doubles swimming in a micro-fluidic channel along with their swimming path are shown in Figure B3. *Dreyfus et al. (2005)* attached a red blood cell to a chain of 1  $\mu\text{m}$  diameter beads to illustrate that the artificial micro-swimmer could be used to transport biological cargo [7].

The artificial micro-swimmer proposed in this whitepaper differs significantly from previous devices in its truly micro-scale design and batch surface micromachining process. With a total length of 105  $\mu\text{m}$ , this device is much more practical for biomedical applications than the swimmers constructed by *Fukuda et al. (1994 and 1995)*. Since the human central canal in the spinal cord is about 100 to 150  $\mu\text{m}$  in diameter, this micro-swimmer could possibly be used to navigate the channel [17]. While paramagnetic bead swimmers have performed well in experiments over the past few years, they are currently restricted to laboratory production because of their DNA bead-linking procedures. This micro-swimmer requires no biological preparation, may be fabricated in quantities of one hundred or more swimmers per SUMMiT V<sup>TM</sup> module, and has promising applications in the biomedical field.

## IV. Device Description

The SUMMiT V<sup>TM</sup> module is divided into four quadrants. In clockwise order, beginning from the top left, the quadrants contain: (a) micro-fluidic sealed test lake, (b) micro-fluidic open test lake, (c) additional micro-swimmers and experimental actuators, and (d) micro-fluidic sealed test stream channel. A 2-D view of the entire SUMMiT V<sup>TM</sup> module is shown in Figure B4 in AutoCAD. The primary design for judging is the set of micro-swimmers, experimental swimmer actuators, and the micro-stream channel on the bottom half of the module.

### Basic Micro-swimmer Design

The basic micro-swimmer consists of a rectangular tail and semicircular head modeled after a spermatozoon like that shown in Figure B1. The micro-swimmer tail is primarily responsible for the propulsion of the robot due to its polysilicon-aluminum (poly-Al) bimorph structure. The micro-swimmer head is shaped to reduce fluid drag and to provide a location to secure the micro-swimmer during the fabrication process. When irradiated by microwaves, the aluminum experiences induction heating on the exposed surface, and the temperature of the tail increases significantly. The difference in coefficient of thermal expansion between the aluminum and

polysilicon strips causes the tail to bend out-of-plane. When the microwave radiation is switched off, the tail is cooled by the surrounding fluid and bends back to its original position.

The range of actuation of the tail is optimized by maximizing the length, change in temperature, and difference in coefficient of thermal expansion (CTE) between the two materials. The poly-Al combination was chosen for the tail structure because difference in CTE between the two materials is much higher than that of other material pairs available in the SUMMiT V™ process. Furthermore, the poly-Al combination was selected because the elastic moduli of the two materials are less than that of silicon nitride; a more flexible tail results in more displacement and more efficient swimming. The MMPOLY4 layer was the only mechanical layer used for the tail in order to minimize the stiffness and maximize the displacement range.

The dimensions of the micro-swimmer tail were adapted from that of human spermatozoa due to their well-known ability to swim in the human body. Human spermatozoa are approximately 40  $\mu\text{m}$  in length [5]. The artificial micro-swimmer was designed to be 100  $\mu\text{m}$  to achieve large enough displacements of the tail needed for wave-like motion. Several dimensions were initially considered for the size of the polysilicon and aluminum parts of the tail and were tested with coupled structural-thermal simulations in ANSYS. The SUMMiT V™ design rules, especially the minimum width of the PTNMETAL layer and the minimum enclosure of the PTNMETAL layer by the MMPOLY4 layer, limited the minimum size of the swimmer. The tail structure consists of a 60  $\mu\text{m}$  by 6  $\mu\text{m}$  PTNMETAL strip enclosed by a 100  $\mu\text{m}$  by 10  $\mu\text{m}$  MMPOLY4 strip. As viewed in AutoCAD, the left sides of the PTNMETAL and MMPOLY4 rectangles are joined so that a 40  $\mu\text{m}$  length of polysilicon is free to oscillate when the tail is irradiated by microwaves. 2-D top down, cross-sectional, and 3-D views of the basic micro-swimmer design are shown in Figure B5.

### **Micro-fluidic Lake and Steam Channel**

The operation of the micro-swimmer in a micro-fluidic environment is critical in illustrating the thermally-driven swimming motion, assessing the performance of the swimmer, and improving future designs. Towards these goals, several micro-fluidic environments were designed on the SUMMiT V™ module for integrated use with the micro-swimmer. Two micro-fluidic test lakes and one test stream channel 3.2 mm by 1.4 mm in size and 12  $\mu\text{m}$  deep are placed on the chip. The micro-fluidic lakes and streams have 200  $\mu\text{m}$  thick walls using all the mechanical layers and encased oxide to enclose a 2.6 mm by 0.8 mm rectangular swimming area with rounded ends. Micro-swimmers are placed along the wall within the swimming chamber for ease of use after fabrication. The swimmers are attached by a thin MMPOLY4 strip to the wall that may be broken off by an operator with micro-tweezers. Each of the lakes and the channel contain about 40 swimmers of different dimensions for testing. 2-D top, cross-sectional, and 3-D views of the sealed micro-lake and micro-channel are shown in Figures B6 and B7.

The swimming areas in the micro-lake and micro-channel on the left side of the module are left open in the SUMMiT V™ design so that their tops may be sealed by a single piece of Plexiglas. Transparent Plexiglas bonded to the top of the micro-lake and micro-channel would allow the operator to view the micro-swimmers moving around the swimming areas. A Plexiglas plate could be bonded to the polysilicon walls of the lake and channel using a silicone adhesive as

reported in other MEMS applications [13]. The fluid flow needed for the micro-channel is accomplished by means of an inlet and an outlet with 300  $\mu\text{m}$  diameter cut from the backside of the wafer. Plastic tubes may be bonded to the inlet and outlet holes with an adhesive to provide a stream of water. The swimming area within the micro-channel will provide a test environment with an adjustable fluid flow rate for demonstration and study of the swimmer's operation in an environment with external flow. Fluid may be dispensed into the swimming area of the open test lake for experiments involving drops of fluid, foreign objects, and swimming near the fluid surface.

### **Additional Micro-swimmer Designs**

The basic micro-swimmer design involves a polysilicon-aluminum strip with a simple semicircular head that is broken-off manually by the operator. Three additional swimmer release mechanisms were designed as well as a micro-swimmer using an experimental nitride-polysilicon bimorph. As in the basic design, the release mechanisms secure the swimmer during the fabrication release process and transportation of the chip.

The second type of micro-swimmer is similar to the basic design already discussed except for the release mechanism. The swimmer head is attached to a 3  $\mu\text{m}$  wide MMPOLY4 beam between two substrate bondpads by a 2  $\mu\text{m}$  wide strip also in MMPOLY4. When a few volts are applied between the bondpads, the narrow strip connecting the swimmer head and beam will melt due to very high localized Joule heating. The third type of micro-swimmer incorporates a thermally-actuated latch system similar to that submitted by the University of Oklahoma in 2007 [4]. Two Chevron or V-shaped thermal actuators are positioned so that the application of a voltage will cause the shuttle to move the jacking system drive away from the micro-swimmer. The head is modified from the basic design to include a MMPOLY3 and MMPOLY4 extension attached to the original bimorph strip. Two 2.5  $\mu\text{m}$  wide arms in MMPOLY2 and MMPOLY4 grip the part of the head in MMPOLY3. The fourth additional micro-swimmer type creates a symmetric head by independently fabricating pieces of the head on the MMPOLY3 layers in the plane of the chip. After fabrication, a specially developed transmission powered by thermal actuators rotates the parts of the head and swimmer tail perpendicular to the chip and snaps the two head parts together. The 3-D symmetric head shape may have desirable hydrodynamic properties that other micro-swimmer flat head shapes. 2-D top, cross-sectional, and 3-D views of the additional types of micro-swimmers are shown in Figures B8 through B10.

The concept for the experimental nitride-polysilicon micro-swimmer is similar to that of the basic polysilicon-aluminum swimmer; a difference in coefficient of thermal expansion between the materials causes the swimmer tail to bend out-of-plane. Both silicon nitride and polysilicon are dielectrically heated by the application of microwave radiation. The nitride-poly swimmer has an advantage over its poly-Al counterpart because the SUMMiT V™ design rules allow for a 3  $\mu\text{m}$  wide swimmer. The fabrication of the nitride-poly swimmer is accomplished by specific NITRIDE\_CUT geometries that remove the nitride material around a thin strip and expose the thermal oxide layer. During the release process, the thermal oxide is etched away and the nitride strip is separated from the substrate. A strip of MMPOLY0 is attached on top of the nitride strip to form the bimorph structure. The nitride-poly swimmer shown in the design has a total length

of 101  $\mu\text{m}$  and width of 3  $\mu\text{m}$ . 2-D top, cross-sectional, and 3-D views of the nitride-poly micro-swimmer are shown in Figure B11.

### **Experimental Actuators**

Since polysilicon-aluminum thermal actuators powered by microwaves are a new development for the SUMMiT V™ process, this design incorporates experimental actuators for testing and measurement. Polysilicon-aluminum actuators using MMPOLY4 and PTNMETAL bend out-of-plane when irradiated by microwaves; however, out-of-plane measurement for SUMMiT V™ devices is more complicated than in-plane measurement. The experimental actuators are rotated 90° in-plane by a thermally-actuated transmission previously developed by the University of Oklahoma [4]. After rotation, the poly-Al bimorph will bend in the plane of the chip and will be easily viewable by the operator. Measurement guides separated by 1  $\mu\text{m}$  are placed next to the actuators for reference. 2-D top, cross-sectional, and 3-D views of one of the cantilever style actuators with transmission are shown in Figure B12.

### **SUMMiT V™ Strengths**

The SUMMiT V™ process makes this artificial micro-swimmer device feasible because of the availability of four mechanical layers, favorable properties of CVD aluminum, and nature of a batch production process. The coefficient of thermal expansion of aluminum is about ten times higher than that of polysilicon and five times higher than that of silicon nitride. Significant bending of the micro-swimmer tail is made possible because of the large CTE of aluminum and large difference in CTE between aluminum and polysilicon. In contrast to biological laboratory methods used to fabricate other artificial micro-swimmers, the SUMMiT V™ process can produce large quantities of micro-swimmers in batches. Depending upon the size of the micro-swimmers, hundreds or thousands of swimmers may be fabricated on a single SUMMiT V™ module. The ability to produce large quantities of micro-swimmers could significantly decrease their cost and increase their availability for MEMS and biological research in the future.

### **Educational Demonstrations**

The micro-swimmer described in this whitepaper could benefit K-12 through post-secondary education in the fields of microbiology, human anatomy and physiology, and fluid mechanics. The motion of the swimmer tail is similar to that of spermatozoa, tadpoles, and some bacterial flagella; the micro-swimmer could be used to introduce the field of swimming motions in biology to K-12 students. Because the micro-swimmer provides the potential application of swimming inside the human body, elementary and middle school teachers could use the concept of a micro-swimmer to educate children about the inner workings of the human body. The micro-fluidic lakes and stream channel are designed for educational demonstrations as well. With a microscope, students could observe many of the micro-swimmers moving around in the micro-lakes or the experimental actuators moving back and forth. This technology would certainly interest junior high and high school students in micro- and nanotechnology and would provide universities an entertaining way to promote engineering to prospective students. At the university level, students could perform experiments with the micro-swimmers furthering their potential application in biomedicine and other fields.

## V. Principle of Operation

### Device Operation

After fabrication, the micro-swimmers are fully assembled but remain attached to the micro-lake walls, snap-off beams, or latch systems. The micro-lakes should be filled with water or another fluid while the plastic inlet and outlet tubes for the micro-channel should be bonded to the backside of the substrate wafer. Both the micro-lake and the micro-channel on the left side of the module should be modified by bonding a Plexiglas plate with a silicone adhesive or other means to the top of the walls. For the basic or mechanical snap-off type, the swimmers can be broken off of the micro-lake or micro-channel walls with a pair of micro-tweezers. The thermal snap-off type may be released by applying a few volts between the appropriate bondpads with a DC power supply and current limiter. On the latch system, the two thermal actuators holding each micro-swimmer require 6.2 V and 14.4 mA between the appropriate bondpads.

In order to operate the micro-swimmers, a directional microwave power source with a density of  $1 \text{ W/mm}^2$  is focused on the area around the swimmers. To avoid excess microwave radiation, the beam should be focused to as small an area as possible, such as 0.5 mm by 0.5 mm. Because oscillation of the swimmer tail relies upon cyclic heating and cooling, the microwave radiation must be applied in a modified square waveform shown in Figure C5 in Appendix C. Based upon simulations in ANSYS, the power should be applied for 0.02 s and should be switched off for the following 0.18 s for each cycle. The necessary waveform may be generated using a function generator or computer-controlled system with an AC power supply. The possible harmful effects of microwave radiation used for the device are currently being considered with calculations reported in Appendix C. If microwave radiation proves to be harmful in any way, oscillating magnetic fields like those used by *Tierno et al. (2008)* may be substituted for microwaves [16].

### Device Measurements

The primary measurement of the micro-swimmer during operation will be performed by the operator visually at a MEMS probe station. After the swimmer is released from the latch system and the microwave power is applied, the operator may observe the swimmer as it travels on the surface of the chip. However, a CCD camera with motion tracking system like that used to observe magnetic bead swimmers by *Tierno et al. (2008)* may be used to record and analyze the position of the swimmer with time [16]. The displacement of the experimental actuators can be measured visually by the  $1 \text{ }\mu\text{m}$  reference markings near the tip of the actuators. The temperature of the swimmer may be an important variable to study during experiments although the movement of the swimmer prohibits the use of tethered temperature measuring device. Infrared imaging like that described in *Baker et al. (2004)* to measure stationary thermal actuators could be adapted for use with the micro-swimmer device described in this whitepaper [1].

## VI. Modeling

Modeling of this unique artificial micro-swimmer incorporates the fields of solid mechanics, heat transfer, fluid mechanics, and electromagnetic radiation. A number of calculations were performed to estimate the heating effect of microwave radiation on the poly-Al strip, structural

response of the strip, and motion of the swimmer based upon analytical models. However, the true multidisciplinary nature of the operation of the swimmer required transient, coupled structural-thermal simulations. The 2-D simulations performed in ANSYS illustrate that the operation of the swimmer is feasible and estimate the related swimming parameters.

When electromagnetic plane waves irradiate the surface of a perfect conductor, they are perfectly reflected and induce currents on the surface of the conductor due to Faraday's Law of Induction [3, 6]. Actual materials like the CVD aluminum used in the SUMMiT V™ process are not perfect conductors and have a finite electrical resistance. As a result, incident electromagnetic waves penetrate a certain distance depending upon the material resistivity and frequency of the radiation. After the power absorbed by the micro-swimmer was calculated, the swimmer tail was modeled in 2-D using ANSYS 11.0 on a Windows XP 64-bit computer with transient, coupled structural-thermal simulations. The basic micro-swimmer with a 100  $\mu\text{m}$  by 10  $\mu\text{m}$  MMPOLY4 strip and 60  $\mu\text{m}$  by 6  $\mu\text{m}$  PTNMETAL strip was used as the baseline case for the calculations because of its similar dimensions to actual spermatozoa. Calculations for the baseline swimmer and parameterization studies concerning the dimensions of the micro-swimmer and microwave power density were conducted and are discussed in Appendix C.

The basic mechanics of flagellar motion are described analytically by *Higdon (1979)* and other authors and may be applied to the micro-swimmer simulation data to predict the swimming speed [10-12, 14]. The calculations shown in Appendix C for the 100/60  $\mu\text{m}$  poly-Al micro-swimmer estimate the swimming speed to be 4.1  $\mu\text{m}/\text{s}$ . Although this swimming speed may appear low with respect to the dimensions of the artificial micro-swimmer, it is about the same as that observed by magnetic bead doublets in other experiments [16]. The estimated swimming speed should be high enough to observe in a micro-fluidic channel visually and/or with a CCD camera and motion tracking system. The combined analytical and numerical model of the micro-swimmer operation illustrates that the device is physically feasible.

## VII. Summary

The artificial MEMS micro-swimmer and micro-fluidic environment designed for the SUMMiT V™ process described in this whitepaper is the first of its kind in scale and ability to be produced by a batch surface micromachining process. The simple swimmer geometry is modeled after human spermatozoa and has a size of approximately 100  $\mu\text{m}$  by 10  $\mu\text{m}$  by 3  $\mu\text{m}$ . Several micro-swimmers are designed to be fabricated in two micro-lake and one micro-channel environments for demonstration of the swimmer's performance. The device's swimming motion is powered by cyclic induction heating of a polysilicon-aluminum bimorph strip from a microwave power source. A 2-D combined analytical and numerical model of the micro-swimmer in ANSYS reported a swimming beat frequency and amplitude of 5 Hz and 0.49  $\mu\text{m}$  respectively. The estimated average swimming speed was determined to be 4.1  $\mu\text{m}/\text{s}$  from analysis of flagellar propulsion reported in the literature. Experimental actuators included in the design may be used to perform sample measurements of the deflection of poly-Al actuators excited by microwave energy in the future. This micro-swimmer has several exciting potential applications such as remote operation and drug delivery in the human body. In addition, the device serves as a fascinating demonstration for K-12 and postsecondary education in the fields of biology, fluid mechanics, and human anatomy and physiology.

## Appendix A: References

- [1] M. S. Baker, R. A. Plass, T. J. Headley, and J. A. Walraven, "Final Report: Compliant Thermo-Mechanical MEMS Actuators LDRD #52553," Sandia National Laboratories, Albuquerque, NM and Livermore, CA, USA, SAND2004-6635, 2004.
- [2] C. J. Brokaw, "Demonstration of microtubule sliding in a beating flagellum," [Online]. Available: <http://www.its.caltech.edu/~brokawc/Demo1/BeadExpt.html>.
- [3] A. B. Bronwell and R. E. Beam, *Theory and Application of Microwaves*, New York: McGraw-Hill, 1947.
- [4] Z. Butler, S. Camp, J. Dingeldein, A. Mann, S. Thompson, A. Watt, and H. Stalford, "Parvissimus Bracchius," Sandia National Laboratories University Alliance Design Competition, University of Oklahoma, 2007. [Online]. Available: [http://mems.sandia.gov/ua/07-doc/OU\\_NovelDesign\\_Whitepaper.pdf](http://mems.sandia.gov/ua/07-doc/OU_NovelDesign_Whitepaper.pdf).
- [5] K. Cui, "Size differences between human X and Y spermatozoa and prefertilization diagnosis," *Molecular Human Reproduction*, vol. 3, no. 1, pp. 61-67, 1997.
- [6] J. Davies and P. Simpson, *Induction Heating Handbook*, London: McGraw-Hill, 1979.
- [7] R. Dreyfus et al., "Microscopic artificial swimmers," *Nature*, vol. 437, no. 6, pp. 862-865, 2005.
- [8] T. Fukuda et al., "Mechanism and swimming experiment of micro mobile robot in water," *MEMS '94 Proc. IEEE*, pp. 273-278, 1994.
- [9] T. Fukuda et al., "Steering mechanism and swimming experiment of micro mobile robot in water," *MEMS '95 Proc. IEEE*, pp. 300-305, 1995.
- [10] J. Gray, "The movement of sea-urchin spermatozoa," *J. Exp. Biology*, vol. 32, pp. 775-801, 1955.
- [11] J. Gray and G. J. Hancock, "The propulsion of sea-urchin spermatozoa," *J. Exp. Biology*, vol. 32, pp. 802-814, 1955.
- [12] J. J. L. Higdon, "A hydrodynamic analysis of flagellar propulsion," *J. Fluid Mech.*, vol. 90, no. 4, pp. 685-711, 1979.
- [13] A. Jain, D. W. Greve, and I. J. Oppenheim, "A MEMS transducer for ultrasonic flaw detection," *International Symposium on Automation and Robotics in Construction*, 2002.
- [14] M. J. Lighthill, "Hydrodynamics of aquatic animal propulsion," *Annual Rev. Fluid Mech.*, vol. 1, pp. 413-446, 1969.
- [15] H. Puschner, *Heating with Microwaves: Fundamentals, Components, and Circuit Technique*, New York: Springer-Verlag, 1966.
- [16] P. Tierno et al., "Magnetically actuated colloidal microswimmers," *J. Phys. Chem. B*, vol. 112, pp. 16525-16528, 2008.
- [17] P. L. Williams et al., Ed., *Gray's Anatomy*, 37<sup>th</sup> ed., New York: Churchill Livingstone, 1989.

## Appendix B: Figures

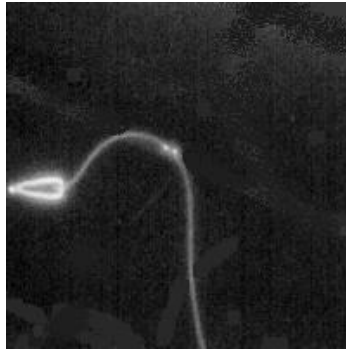


Figure B1: Picture of Spermatozoon at Beginning of Swimming Cycle [2]

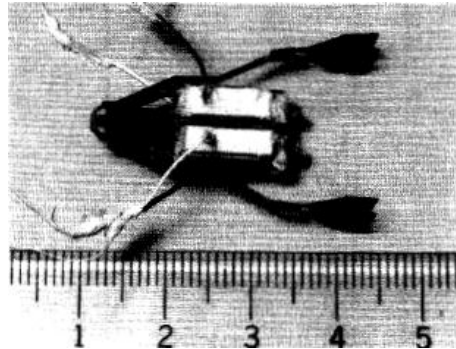
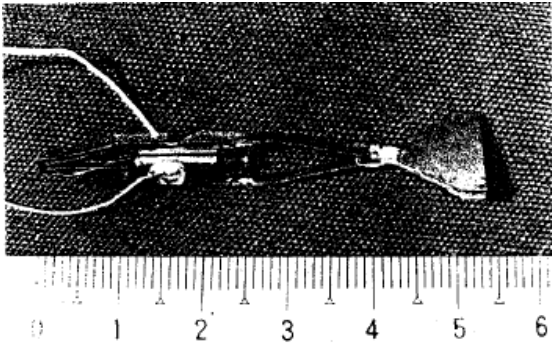


Figure B2: Millimeter scale swimmer (a) without steering controls and (b) with steering controls [8-9]

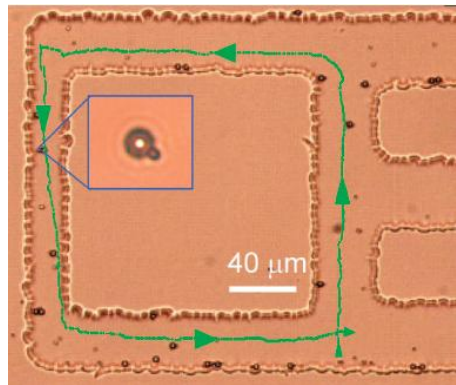
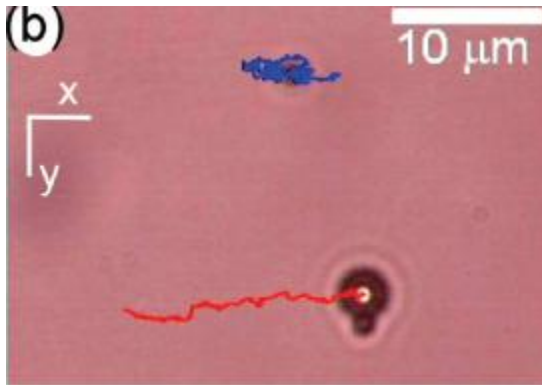


Figure B3: (a) Individual Magnetic Doublet and (b) Multiple Doublets in Micro-fluidic Channel [16]

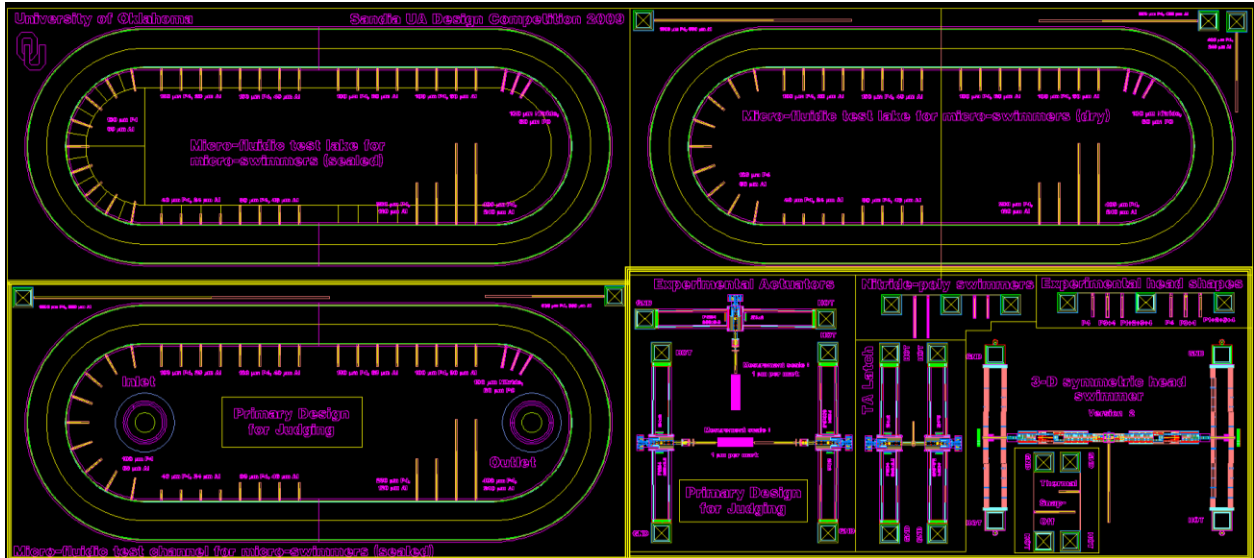


Figure B4: View of Entire SUMMIT V™ Module in AutoCAD



Figure B5 (a): 2-D Top View of Basic Micro-swimmer



Figure B5 (b): Horizontal Cross-sectional View of Basic Micro-swimmer

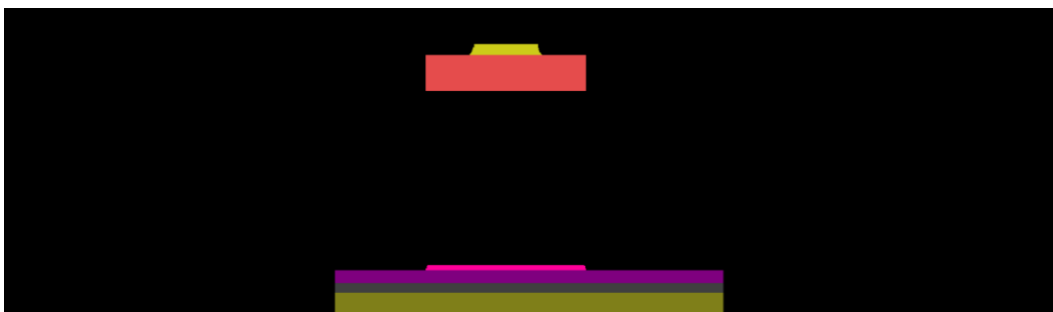


Figure B5 (c): Vertical Cross-sectional View of Basic Micro-swimmer



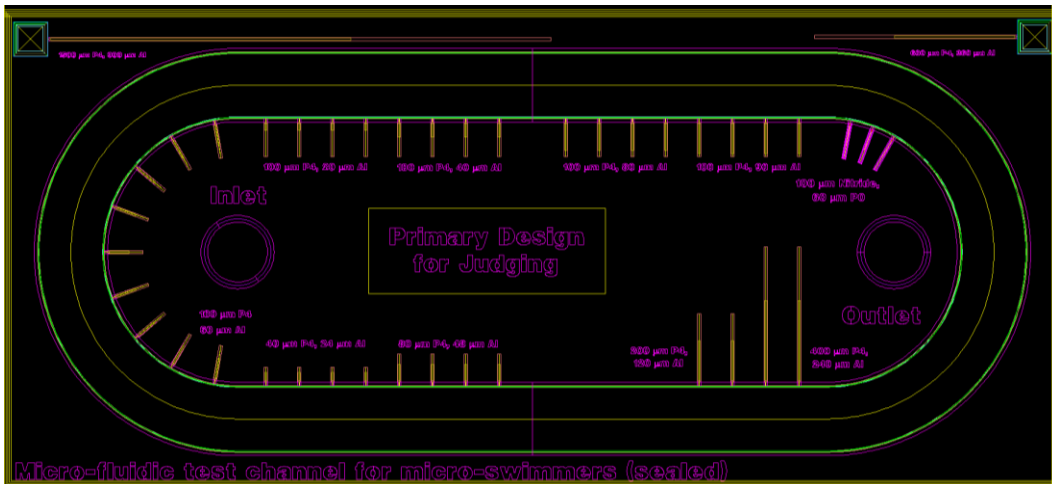


Figure B7 (a): 2-D Top View of Sealed Micro-channel

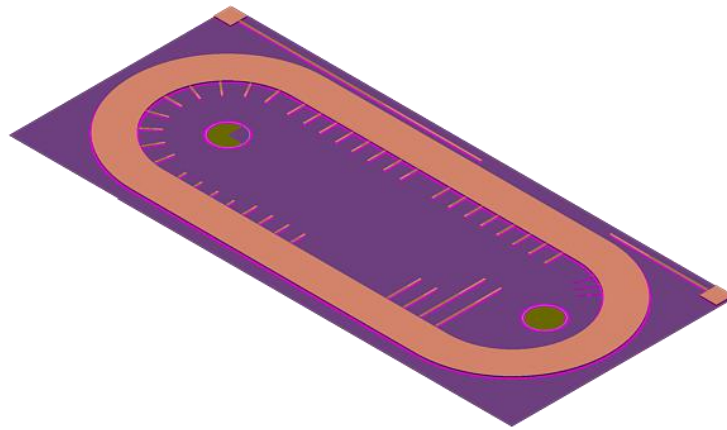


Figure B7 (b): 3-D View of Sealed Micro-channel

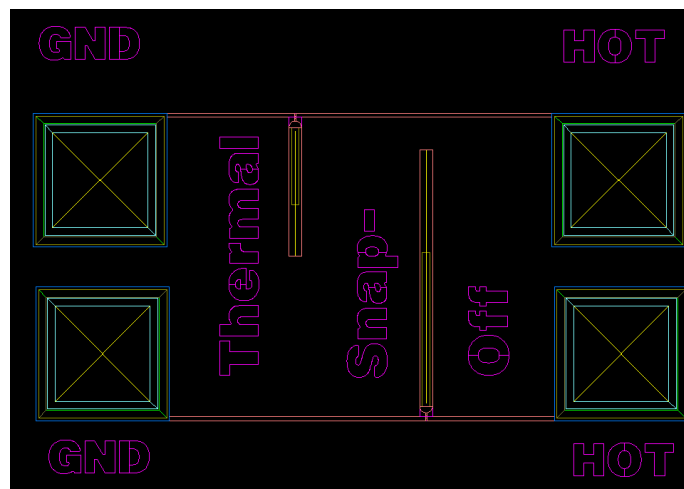


Figure B8 (a): 2-D Top View of Thermal Snap-off Micro-swimmer



Figure B8 (b): Cross-sectional View of Thermal Snap-off Micro-swimmer through Beam

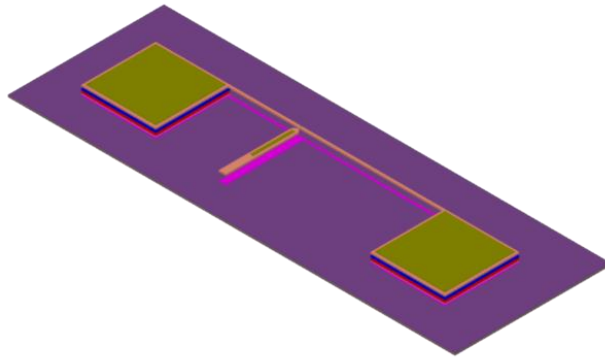


Figure B8 (c): 3-D View of Thermal Snap-off Micro-swimmer

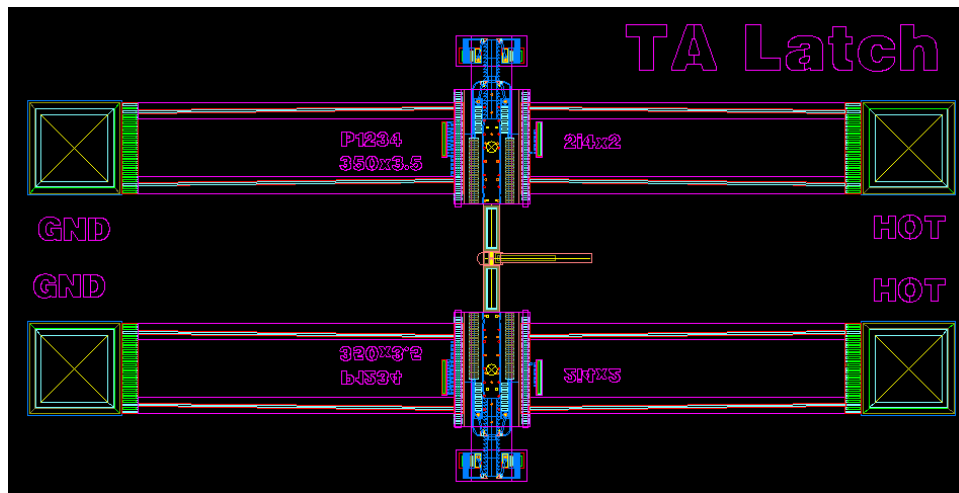


Figure B9 (a): Top View of Latch Mechanism Micro-swimmer



Figure B9 (b): Lengthwise Cross-sectional View of Latch Mechanism Micro-swimmer

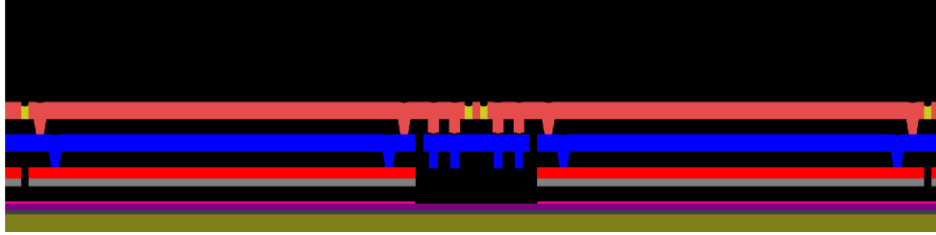


Figure B9 (c): Cross-sectional View of Latch Mechanism Micro-swimmer through Latch Arms

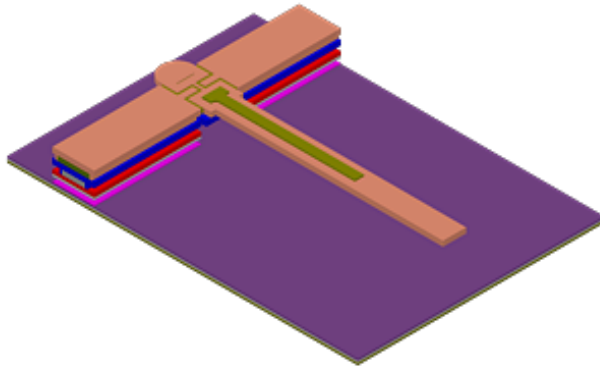


Figure B9 (d): 3-D View of Latch Mechanism Micro-swimmer (Thermal Actuators Removed)



Figure B10 (a): Top View of Swimmer with 3-D Symmetric Head

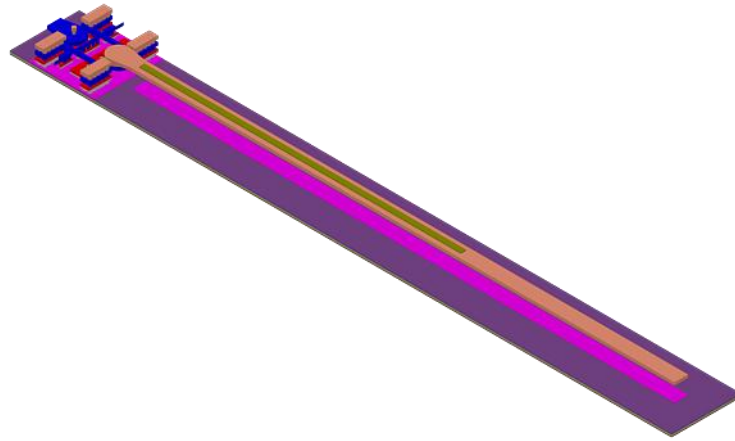


Figure B10 (b): 3-D View of Swimmer with 3-D Symmetric Head



Figure B11 (a): Top View of Nitride-polysilicon Micro-swimmer



Figure B11 (b): Horizontal Cross-sectional View of Nitride-polysilicon Micro-swimmer



Figure B11 (c): Vertical Cross-sectional View of Nitride-polysilicon Micro-swimmer

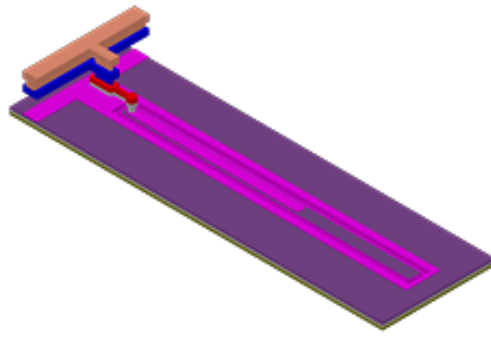


Figure B11 (d): 3-D View of Nitride-polysilicon Micro-swimmer

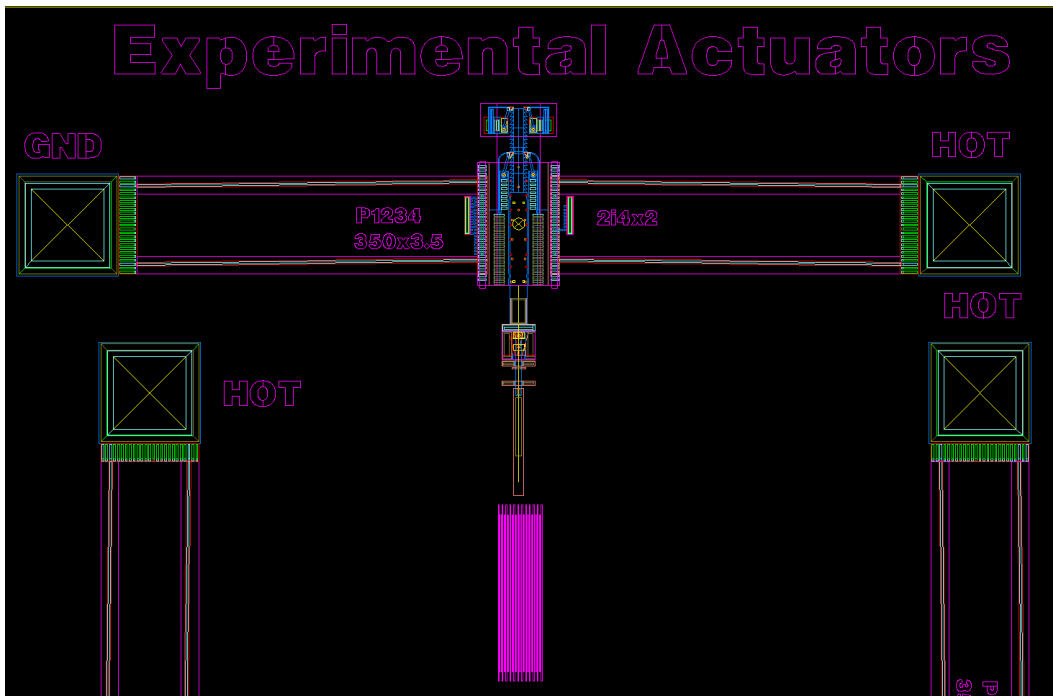


Figure B12 (a): Top View of Experimental Actuator

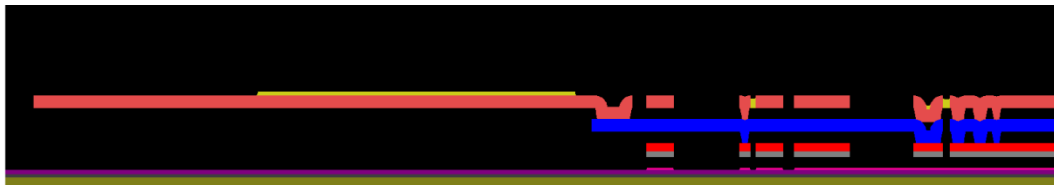


Figure B12 (b): Vertical Cross-sectional View through Center of Experimental Actuator

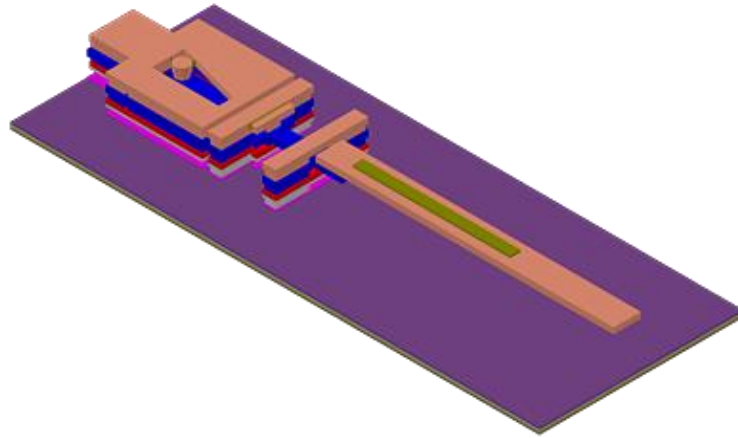


Figure B12 (c): 3-D View of Experimental Actuator (External Thermal Actuator Excluded)

## Appendix C: Calculations

### Microwave Power Source

The amount of microwave power absorbed by the aluminum strip depends heavily on the depth of penetration of the incident microwaves, which is itself dependent upon the frequency of radiation. The skin depth or depth of penetration  $\delta$  is defined as

$$\delta = \sqrt{2\rho/\mu\omega} \quad (\text{Eq. 1})$$

where  $\rho$  is the electrical resistivity and  $\mu$  is the magnetic permeability of the material and  $\omega$  is the radian frequency of the incident radiation [3, 6]. For aluminum with magnetic permeability  $\mu \approx \mu_0$  of  $4\pi \times 10^{-7}$  A/m and resistivity of  $2.88 \times 10^{-8}$   $\Omega/\text{m}$  at  $40^\circ\text{C}$ , the skin depth versus radiation frequency was calculated and is shown in the figure below.

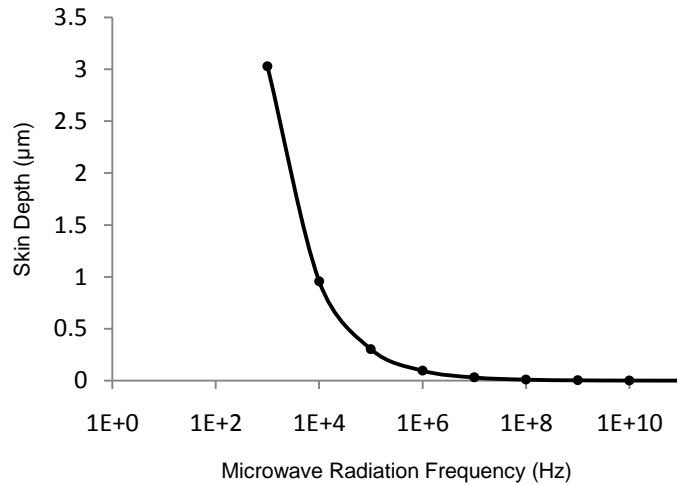


Figure C1: Plot of Skin Depth vs. Frequency for Microwave Radiation

The power absorbed by the aluminum strip decays exponentially with distance from the surface of the strip; the resultant heat generated in the material decays to 5% of its value at the distance  $3\delta$  from the surface. For depths of penetration much less than the thickness of the material, induction heating of metals by microwaves is largely a surface effect. The magnitude of the absorbed power of the conductor within the skin depth is dependent upon the skin depth and the radiation power density; increased radiation frequency results in higher power absorption and more rapid heating of the strip. The power absorbed by the conductor per unit area is given by

$$P_a = \rho H_{0,max}^2 / 2\delta \quad (\text{Eq. 2})$$

where  $H_{0,max}$  is the magnetic field strength calculated from the microwave power intensity. A plot of the absorbed microwave power versus radiation frequency is shown below for the PTNMETAL aluminum strip.

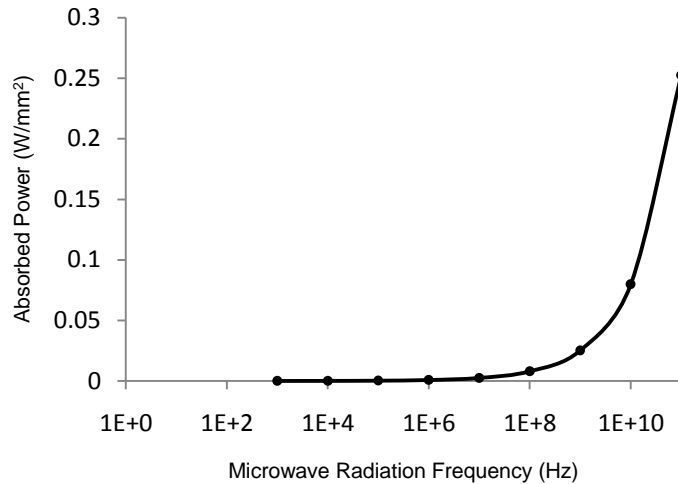


Figure C2: Plot of Absorbed Microwave Power versus Radiation Frequency

The radiation power density and frequency were chosen to be  $1 \text{ W/mm}^2$  and  $10 \text{ GHz}$  respectively because of the need to provide rapid heating of the swimmer tail with radiation in the microwave range. At the specified radiation intensity and frequency, the estimated power absorbed per unit area of the micro-swimmer tail is  $0.08 \text{ W/mm}^2$ .

### ANSYS Multiphysics Simulations

Because of the complexity of the transient, coupled structural-thermal model required to simulate the device, FEA simulations were performed on a 2-D model. The poly-Al tail strip was modeled in ANSYS by two adjacent rectangular areas with quadrilateral meshes. The microwave power irradiated on the aluminum surface was treated as uniform internal heat generation in the first row of elements in the aluminum area on the side exposed to microwaves. The side of the polysilicon area was restrained from moving by imposing displacement boundary conditions. Heat transfer to the water around the swimmer tail was modeled as convection with an ambient temperature of  $37^\circ\text{C}$ ; convective heat transfer coefficients were estimated by assuming the temperature profile of the water surrounding the swimmer tail decayed exponentially with distance away from the swimmer. Non-linear, transient effects were considered in the simulation due to the complex and time-dependent nature of the swimmer's operation. The 2-D model of the poly-Al micro-swimmer tail in ANSYS is shown in the figure below.

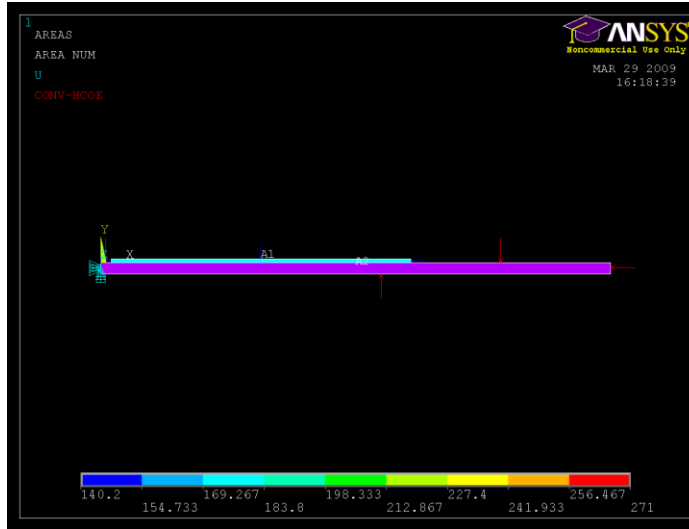


Figure C3: 2-D Model of Poly-Al Micro-swimmer Tail in ANSYS

Results from the ANSYS multiphysics simulation for the baseline 100/60  $\mu\text{m}$  poly-Al strip show that the tip of the aluminum attains a maximum displacement of 0.97  $\mu\text{m}$  after 0.02 s and a maximum temperature of 145°C. Over the remaining 0.18 s in the swimming cycle, the swimmer returns to near its original position and temperature. Since the bending of the aluminum strip drives the oscillation of the unsupported 40  $\mu\text{m}$  polysilicon tail length, the estimated amplitude of the tail beat is equal to half of the maximum displacement of the aluminum strip. Therefore, the predicted beat frequency and amplitude of the swimming motion is 5 Hz and 0.49  $\mu\text{m}$ . The plots of vertical displacement and temperature at the end of the heating part of the cycle for the baseline poly-Al strip at 0.02 s are shown in the figures below.

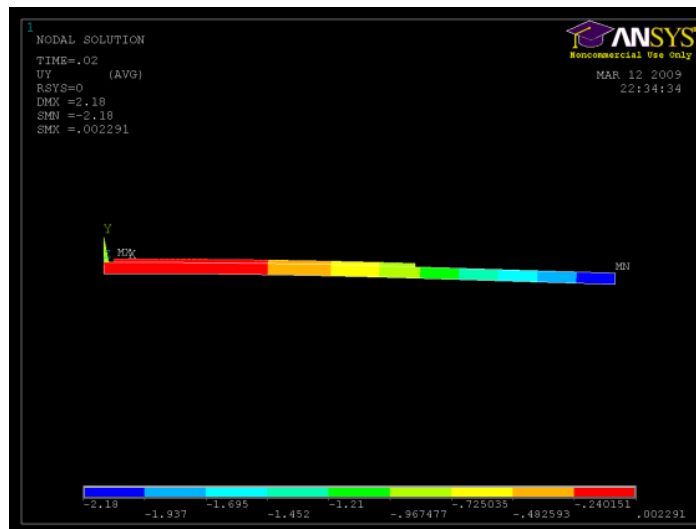


Figure C4 (a): Plot of Vertical Displacement of Baseline Poly-Al at 0.02 s

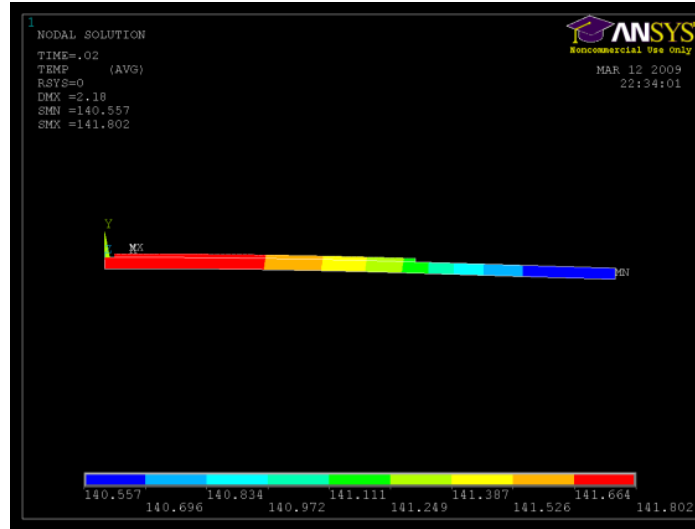


Figure C4 (b): Plot of Temperature of Baseline Poly-Al at 0.2 s

As indicated by the deformed shape of the poly-Al strip in the figures above, a bimorph strip is only capable of bending in one direction if the temperature does not go below the ambient. Therefore, the beat of the poly-Al bimorph tail is inherently one-sided. The analytical model of flagellar propulsion developed by *Higdon (1979)* assumes a true sinusoidal wave form [12]. For the purposes of estimation, the amplitude of the transverse wave in the analytical model was assumed to be equal to half of the one-sided amplitude of the poly-Al bimorph. Based upon the single cycle simulation for the baseline case, a five cycle transient simulation was performed for the same dimensions and microwave power density to illustrate the operation of the swimmer over a time period of 1.0 s. The modified square wave function describing the time-dependent microwave radiation and heat generation in the ANSYS model is shown in the figure below. The square wave function consists of alternating periods of switching on the microwave source at  $1 \text{ W/mm}^2$  for 0.02 s and switching off the microwave source for 0.18 s.

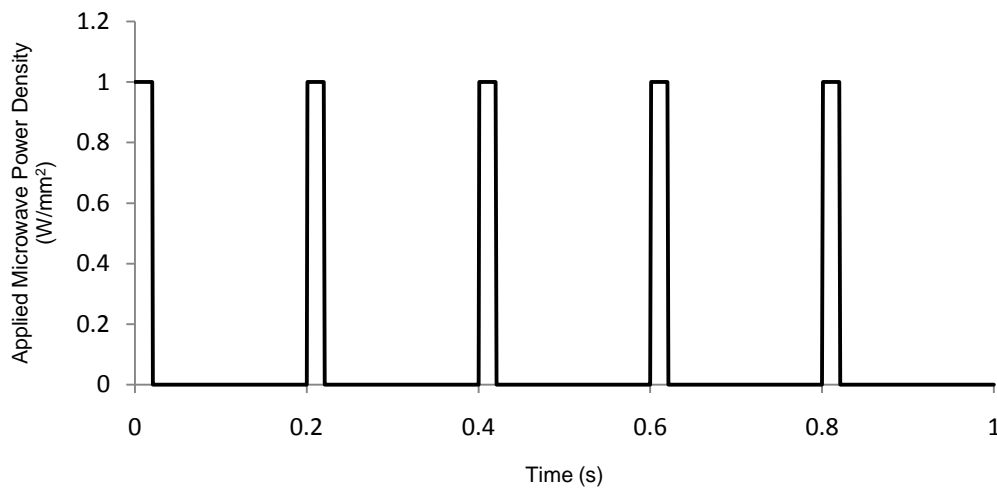


Figure C5: Time-dependent Microwave Power Wave Function for 1.0 s

Plots of the aluminum tip displacement and temperature versus time are shown in the figures below for the five-cycle, 1.0 s ANSYS simulation.

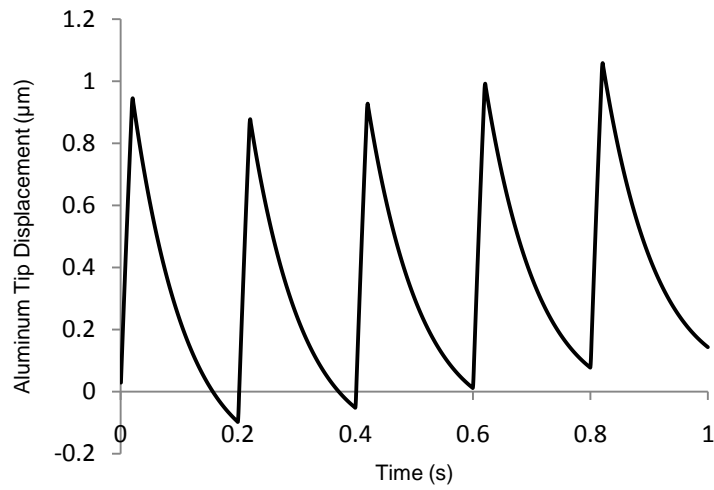


Figure C6 (a): Plot of Tip Displacement versus Time for 1.0 s Simulation

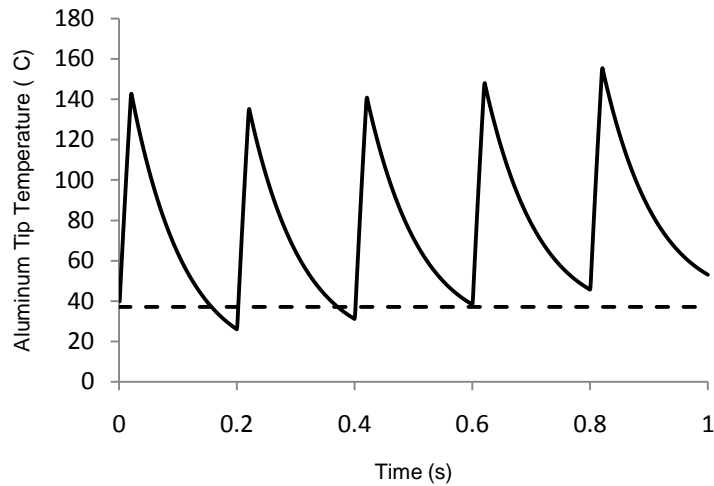


Figure C6 (b): Plot of Tip Temperature versus Time for 1.0 s Simulation

The plots of the displacement and temperature of the tip of the aluminum strip indicated that the single cycle simulation previously presented well represents the periodic behavior of the micro-swimmer tail. The tip displacement at the end of the heating cycles was approximately 1 µm for the simulation conducted for five cycles. Similarly, the temperature increased to a maximum of about 140°C to 150°C at the end of the heating cycle and near the ambient temperature of 37°C at the end of the cooling cycle.

### Fluid Mechanics Analysis

After calculating the periodic behavior of the poly-Al strip used as a micro-swimmer tail, the fluid mechanical properties of the swimmer such as swimming speed may be calculated. The

swimming speed  $U$  of a micro-scale swimmer propelled by a plane-wave flagellum depends upon the transverse wave velocity  $V$  traveling the length of the tail. A graph of the ratio of the swimming speed to wave velocity presented by *Higdon (1979)* was used to estimate the swimming speed based upon the simulation results.

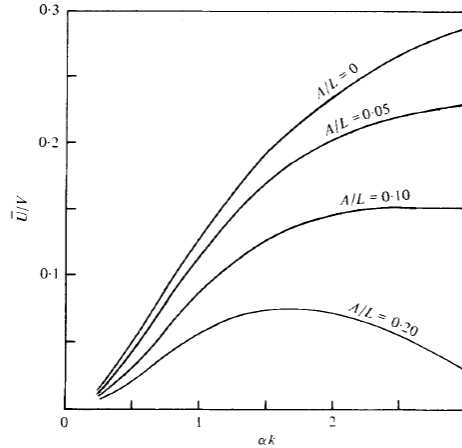


FIGURE 5. Average swimming speed as a function of amplitude  $\alpha k$ . Curves are for an organism without a cell body and for three different head radii  $A$ . Single wavelength,  $N_\lambda = 1$  ( $a/L = 0.01$ ).

Figure C7: Plot of Average Swimming Speed to Wave Velocity Ratio [12]

The vertical axis in the figure above represents the non-dimensional swimming speed while the horizontal axis represents the product of the wave amplitude  $a$  and wave number  $k$ . The swimming speed is highly dependent upon  $\alpha k$  and the geometry of the swimmer. For the baseline 100/60  $\mu\text{m}$  micro-swimmer, the semicircular head has the same thickness as the tail. Therefore, the curve for the head diameter  $A$  to tail length  $L$  ratio of zero was used to estimate the swimming speed. Assuming the tail forms a sinusoidal shape with approximately one-half wavelength, the transverse wave velocity was calculated to be 822  $\mu\text{m/s}$ . Because of the probable inefficiency of the swimming motion illustrated by the transient simulations, the ratio  $U/V$  may be as low as 0.005, resulting in an average swimming speed of 4.1  $\mu\text{m/s}$  [12]. The fluid resistance coefficients described by *Higdon (1979)* and others were not included in the simulations performed in ANSYS because of the difficulty in modeling micro-fluidic behavior with the software. In the future, other multiphysics simulation packages may be used to simulate the combined structural-thermal-fluid environment of the bimorph tail surrounded by liquid.

### Parameterization Studies

Three parameterization studies based upon the 2-D ANSYS models were performed to examine the behavior of the micro-swimmer with changes in the microwave power density and poly-Al swimmer tail dimensions. For all three studies, the simulations were conducted from 0 to 0.02 s because of the time controls in the baseline 100/60  $\mu\text{m}$  case simulation. Micro-swimmers of different sizes were designed in the micro-lakes and micro-channels in the SUMMIT V<sup>TM</sup> module with the dimensions from the two dimensional parameterization studies. Therefore, experiments may be conducted in the future to analyze the accuracy of the combined analytical/numerical model in predicting the behavior of the micro-swimmers.

In the first study, the microwave power density applied by the source was changed while the dimensions of the swimmer were kept constant at the baseline values. In all three parameterization studies, the maximum tip displacement was recorded because it represents the amplitude of the swimmer's tail oscillation. The length of MMPPOLY4 material not covered by aluminum is the part of the tail that will assume a wave motion similar to that of a spermatozoon. Because the thermal diffusivity of both polysilicon and aluminum is very large with respect to the length scales used in the design, the temperature was found to be fairly uniform across the tail in the simulations performed. Therefore, the temperature at the tip of the aluminum strip represents the temperature of the swimmer tail as a whole. Plots of the microwave power source versus the vertical displacement and temperature of the tip of the aluminum strip are shown in the figures below.

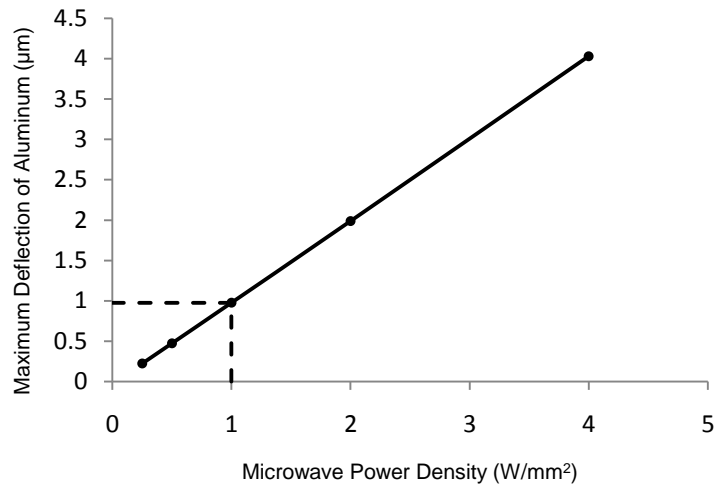


Figure C8 (a): Plot of Vertical Displacement versus Microwave Power Density

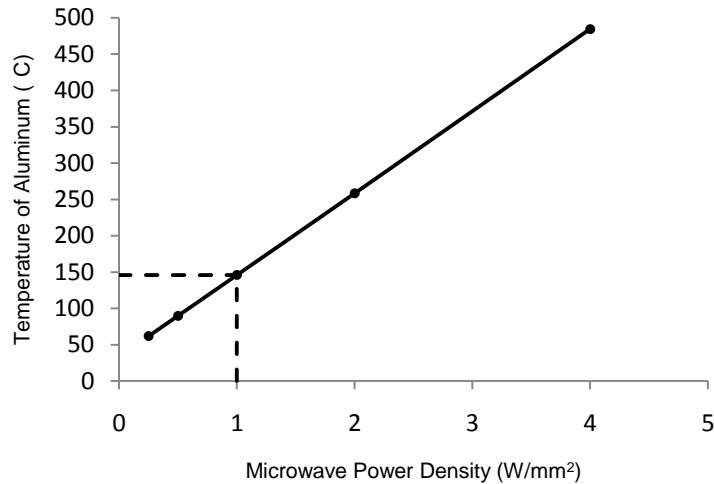


Figure C8 (b): Plot of Temperature versus Microwave Power Density

The plots shown in the figures above indicate that the displacement and temperature of the tip of the aluminum strip increase significantly with increasing microwave power density. While

increased tip displacement will result in increased swimming speed and efficiency, excessive temperatures may result in harmful effects to the surrounding environment. The recommended microwave power density from the baseline case is  $1 \text{ W/mm}^2$ .

The second parameterization study examined the dependence of the aluminum tip displacement and temperature on the length of the aluminum strip for a fixed MMPLY4 length of  $100 \mu\text{m}$ . All other boundary conditions and time controls were kept constant for the second study. Plots of displacement and temperature of the aluminum tip versus length of the aluminum strip at  $0.02 \text{ s}$  are shown in the figures below.

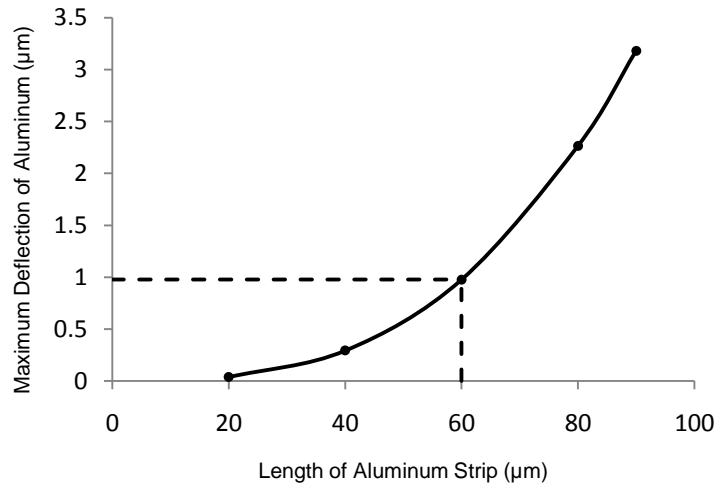


Figure C9 (a): Plot of Tip Displacement versus Aluminum Length

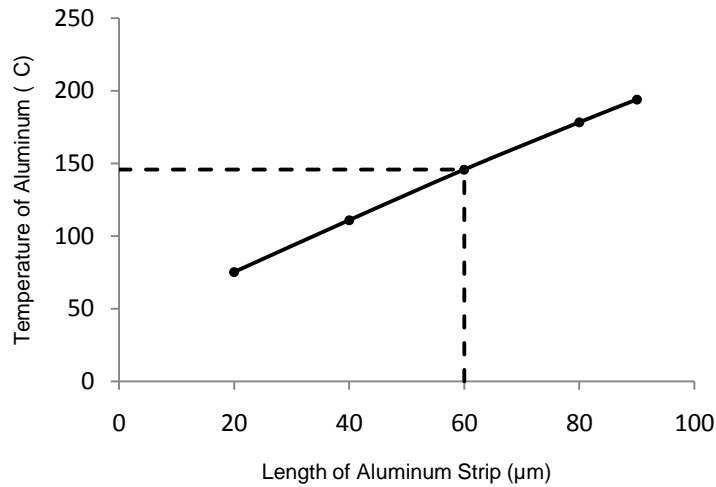


Figure C9 (b): Plot of Tip Temperature versus Aluminum Length

Results from the parameterization study shown in the figures above suggest that the aluminum tip displacement and temperature increase with as the length of the aluminum strip increases relative to the polysilicon strip. A longer aluminum strip with increased surface area absorbs more microwave radiation and expands more because of its increased length. The out-of-plane

bending represented by the tip displacement increases as the aluminum strip expands more and more. The temperature of the strip increases as expected because the amount of power absorbed by the aluminum strip increases relative to the size of the polysilicon strip. The average swimming speed of the swimmer was estimated and plotted versus the length of the aluminum strip in the figure below.

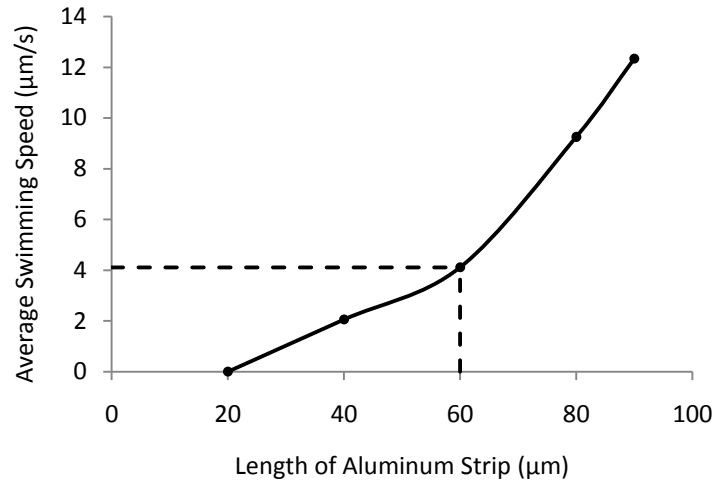


Figure C9 (c): Plot of Average Swimming Speed versus Aluminum Length

The plot of average swimming speed versus the length of the aluminum strip shown in the figure above was created by estimating the ratio  $U/V$  from the chart provided by *Higdon (1979)* and should be considered a rough approximation. The calculation assumes that the tail forms a half wavelength shape for aluminum strip lengths of 20, 40, and 60 µm and a third of a wavelength for aluminum strip lengths of 80 and 100 µm. Based upon this assumption, the optimal speed for the swimmer may still be for the 100/60 µm baseline dimension case. Although the swimming speed does appear to increase for an aluminum strip lengths of 80 and 100 µm in the figure above, the tail may not form the proper shape for swimming if aluminum covers most of the polysilicon strip. The longer length of the aluminum strip results in increased tail displacement, formation of a shorter portion of a complete wavelength, and higher transverse wave speeds. The 60 µm aluminum strip length was still considered optimal to ensure that the tail forms the proper wave-like shape for flagellar propulsion.

The third parameterization study considers the change in behavior of the swimmer as the total length of the tail changes for a fixed ratio of the lengths of the aluminum and polysilicon strips. The ratio of the length of the aluminum strip to the length of the polysilicon strip was held constant at 0.6 (as used for the baseline case) while the overall length of the tail was changed. All time controls and boundary conditions were kept constant for the third parameterization study from the baseline case. Plots of the tip displacement and temperature of the aluminum versus the length of the swimmer tail are shown in the figures below.

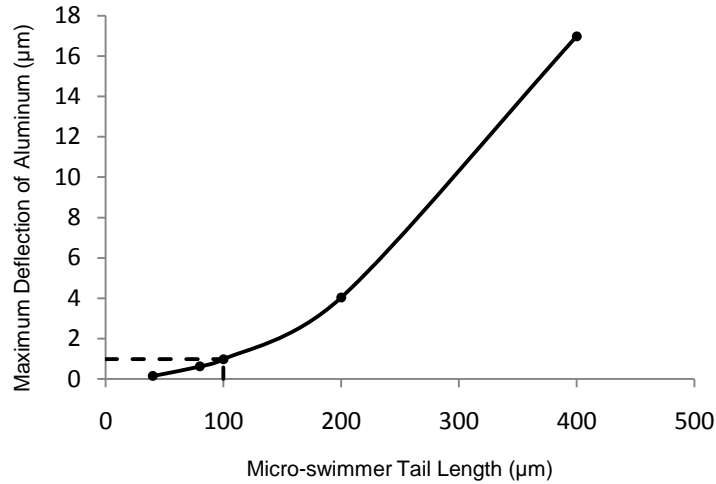


Figure C10 (a): Plot of Tip Displacement versus Tail Length

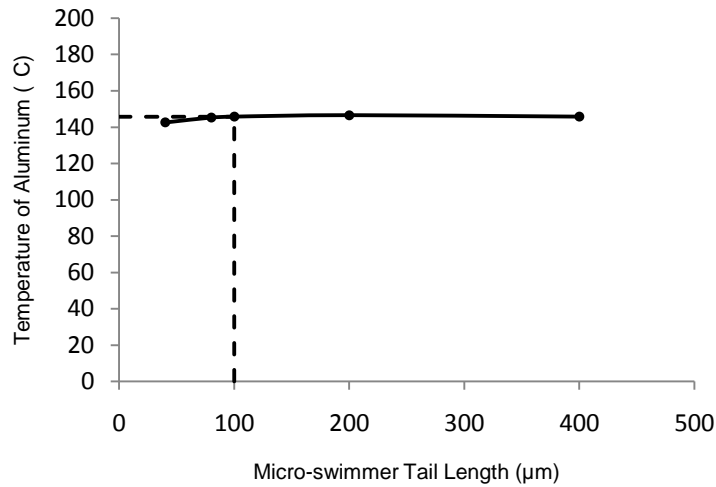


Figure C10 (b): Plot of Tip Temperature versus Tail Length

The third parametric study investigating the effect of varying tail lengths for a constant aluminum to polysilicon length ratio demonstrates that the tip displacement increases significantly with the tail length while the temperature stays almost constant. Increased lengths of the aluminum and polysilicon strips results in larger thermal expansions and increased out-of-plane bending. The fixed aluminum to polysilicon length ratio results in a similar thermal response for the tail lengths studied. The plot of temperature versus tail length shown in Figure C10 (b) indicates that heating effects are similar to micro-swimmers with the same aluminum to polysilicon length ratio. The plot of the estimated swimming speed versus micro-swimmer tail length is shown in the figure below.

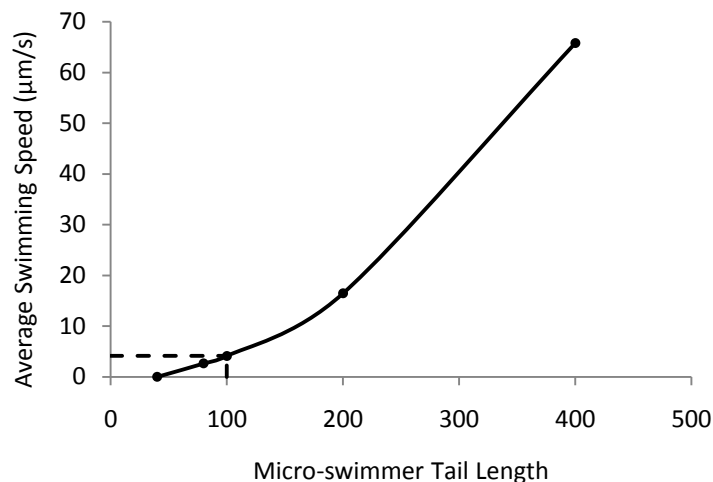


Figure C10 (c): Plot of Average Swimming Speed versus Tail Length

The ratios  $U/V$  for each swimmer tail length described in the figure above were estimated from *Higdon (1979)* as for the other studies performed [12]. The calculations shown in the figure above suggest that the average swimming speed of the micro-swimmer may increase significantly as the length of the tail increases. However, the increase in swimming speed appears to be almost directly proportional to the tail length for the lengths of 100, 200 and 400  $\mu\text{m}$  studied. The magnitude of the swimming speed may increase though the swimming speed relative to the tail length may not increase noticeably. The similar thermal response of the different length tails examined in the third parameterization studied indicates that they may all have beat frequencies close to 5 Hz. Since the oscillating polysilicon part of the tail is equally likely to assume a half wavelength because of the constant aluminum to polysilicon length ratio, the swimming speed may increase as tip displacement of the aluminum strip increases. The performance of the micro-swimmer in applications where the large size of 400  $\mu\text{m}$  long tail is acceptable may be significantly greater than that of spermatozoa-sized swimmers.

### Non-microwave Thermal Actuators

Chevron or V-shaped thermal actuators were used for the swimmer latch mechanism and experimental actuators. In both cases, 350  $\mu\text{m}$  leg length actuators designed by the University of Oklahoma in 2007 were used because of success with prior designs [4]. The thermally-actuated latch system requires a displacement of about 6  $\mu\text{m}$  while the experimental actuator requires about 12  $\mu\text{m}$ . In 2007, the team from the University of Oklahoma calculated the required voltage and current needed to operate the actuators as well as the resultant maximum displacement and peak force. Plots of the actuator force versus displacement and maximum displacement versus voltage and current for the thermal actuators incorporated into the design are shown in the figure below.

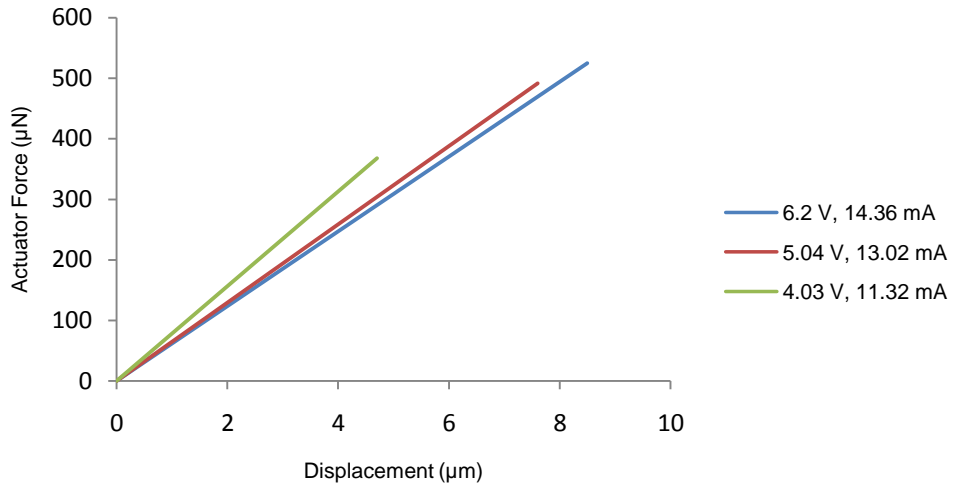


Figure C11 (a): Plot of Thermal Actuator Force versus Displacement

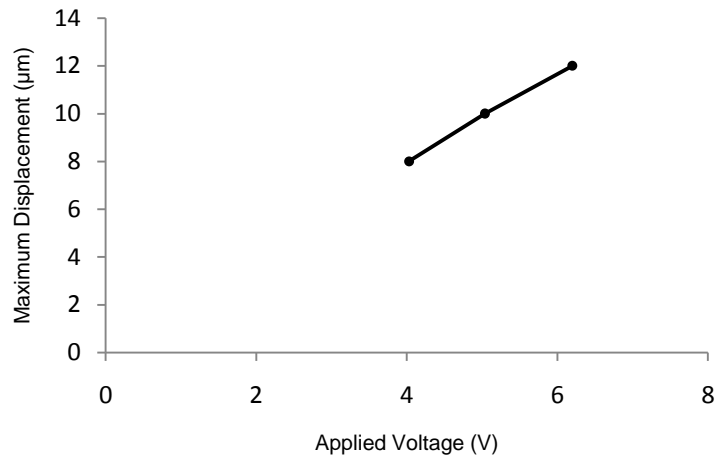


Figure C11 (b): Plot of Thermal Actuator Maximum Displacement versus Applied Voltage

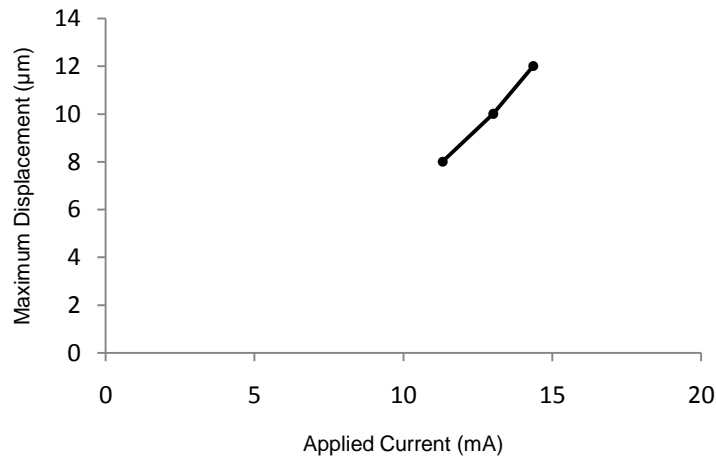


Figure C11 (c): Plot of Thermal Actuator Maximum Displacement versus Applied Current

Calculations used to generate the force versus displacement plot in the figure above demonstrated that the thermal actuators experienced a maximum displacement of 12  $\mu\text{m}$  at 6.2 V and 14.36 mA. Therefore, the thermal actuators used for the latch system and experimental actuator transmission should be operated at these voltage and current values.

## Microwave Safety

Before using microwave radiation to operate micro-swimmers on the surface of a SUMMiT V™ module, the effects of microwave radiation on the human body must be considered. The following calculations are a preliminary consideration of the safety of the proposed microwave power source. In the future, further research will be conducted to more conclusively examine the effects of microwave radiation in this application.

The suggested microwave power density for the operation of the baseline swimmer design is 1  $\text{W}/\text{mm}^2$ . In order to limit the area of exposure, the area irradiated by microwaves should be restricted to 0.5 mm by 0.5 mm. The United States military and several companies have produced guidelines for the maximum permissible amount of microwave radiation for the safety of the person exposed to the radiation. Two plots showing the recommended limit for microwave power density are shown in the figure below [15].

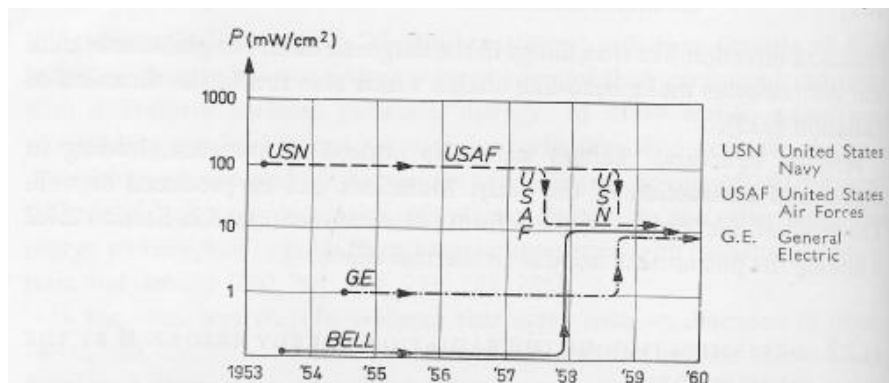


Fig. 177. The maximum permissible energy density of electromagnetic radiation on human beings as established by various American institutes and industries between 1953 and 1960.

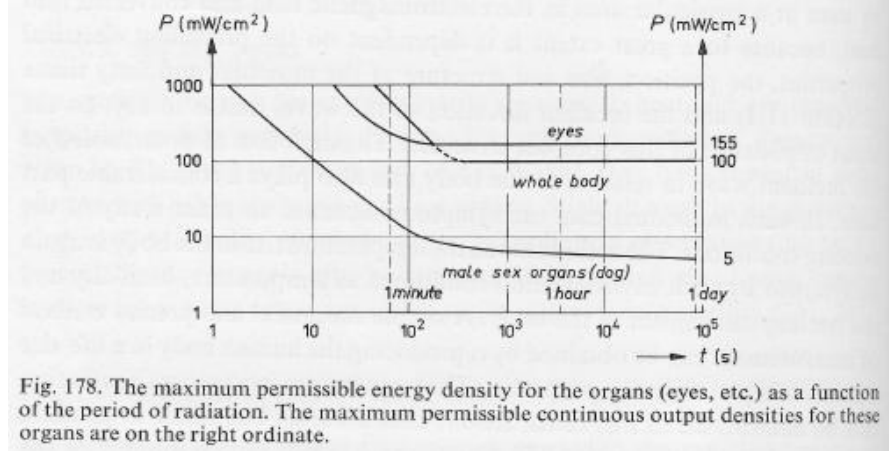


Fig. 178. The maximum permissible energy density for the organs (eyes, etc.) as a function of the period of radiation. The maximum permissible continuous output densities for these organs are on the right ordinate.

Figure C12: Plots of Recommended Maximum Microwave Power Density [15]

The plot at the top of the figure above shows the maximum amount of permissible microwave energy allowed in areas occupied by humans versus the date in years. In the past, the U.S. Air Force and Navy reduced the limit to  $10 \text{ mW/cm}^2$  or  $10^{-3} \text{ W/mm}^2$ . The plot at the bottom of the figure above displays the microwave power density versus the amount of exposure time in seconds. The three curves in the second plot represent the areas of the eyes, whole body, and male reproductive organs. All three data sets indicate that the maximum allowed power density decreases with exposure time. For short exposure times, the maximum power density for safe operation may be greater than  $1000 \text{ mW/cm}^2$  or  $10^{-2} \text{ W/mm}^2$ .

For the case of simple operation of the SUMMiT V™ module, the proposed microwave radiation function is shown in Figure C5. For an interval of 1.0 s, microwave power will only be applied for one-tenth of the time or 0.1 s. Therefore, the effective power density should much less than the actual power density of  $1 \text{ W/mm}^2$ . Safety equipment may also be worn by the operator to reduce the absorbed intensity of the radiation. A table with several types of safety equipment and the known values of permeability by microwaves is shown in the figure below.

TABLE VI

Material	f =	Permeability [%]			
		5.9	9.7	18.8 [Gc/s]	550 [mμ]
Film of gold on plastic of 11 mμ (480 Ω/cm <sup>2</sup> ) 30 mμ (19.2 Ω/cm <sup>2</sup> )		23	10	0.8	49
		0.16	0.1	0.01	24
Film of gold on glass 75 mμ (0.24 Ω/cm <sup>2</sup> ) thick		0.04	0.01	0.004	3.2
Glass 6.5 mm thick		30	25	16	85
Lubice glass 4.8 mm thick		80	50	25	92
Corning glass with conducting layer of 1.5 μ (2.4 Ω/cm <sup>2</sup> )		1.6	1.2	0.08	45
Electropane glass with conducting layer of 0.3 μ (11.2 Ω/cm <sup>2</sup> )		9	10	8	80

Figure C13: Safety Equipment and Permeability Table [15]

The permeability for a thin film of gold on glass listed in the table above is 0.01% for a microwave frequency of 9.7 GHz, close to the proposed 10 GHz value for this device. If a pair of gold coated glasses was worn by the operator, the operator's eyes would only absorb about  $10^{-4} \text{ W/mm}^2$  of radiation from a  $1 \text{ W/mm}^2$  source. Other safety equipment such as garments with metal particles may also be worn for the safety of the operator and shields with high absorption characteristics may be setup around the module.

In potential biomedical applications, the effects of microwave radiation on swimmers inside the human body are not known. Localization of the microwave beam may prevent the patient from absorbing excess radiation though cyclic application of microwave power may have harmful health effects [15]. Before preliminary use of microwave radiation at power levels on the order of  $1 \text{ W/mm}^2$ , the health effects of microwaves must be fully studied. If microwaves are determined to be unsafe for use in human patients, oscillating magnetic fields provided by a solenoid may be used instead. The authors of *Tierno et al. (2008)* applied oscillating magnetic

fields with a simple solenoid to power microscopic swimmers made from paramagnetic beads [16]. A similar technique may be used for in-vivo operation of this MEMS micro-swimmer with the same induction heating effect of the aluminum strip. The safety of microwave radiation will be considering in on-going design improvements to this device.